

Response to comments of Reviewers

Interactive comment on “Hybrid improved EMD-BPNN model for the prediction of sea surface temperature” by Zhiyuan Wu et al.

Anonymous Referee #2

Received and published: 3 February 2019

The authors are grateful to this reviewer for pin-point and pertinent comments and checking the paper. All comments are addressed point by point, each starting with an original comment and followed by a response in italic, as follows.

In this paper, authors discussed the prediction of sea surface temperature. In this paper, an SST predicting method based on improved empirical mode decomposition (EMD) algorithms and back-propagation neural network (BPNN) is proposed. Statistical analysis of the case study demonstrates that applying the proposed hybrid CEEMD-BPNN model is effective for the SST prediction. I recommend this paper to be publicated. And it is better if the authors consider the following mentioned remarks and further improve the manuscript before submitting the final version.

Response: We are grateful to these positive comments.

1. More methods in practical application or commercial application need to be introduced. Which can make this paper more persuasive.

Response: Thank you for your suggestion. As the reviewer said, many noise cancellation methods based on the scale-adaptive remixing and demixing of Intrinsic Mode Functions (IMFs) constructed using Empirical Mode Decomposition (EMD) had been provided in practical application or commercial application. We briefly stated these in the introduction section.

2. The relationship and difference among EMD, EEMD and CEEMD method should be more specific and clear.

Response: Thank you for your suggestion, and we added the following statement to the revised manuscript.

The ensemble empirical mode decomposition (EEMD) method is a noise assisted empirical mode decomposition algorithm. The CEEMD works by adding a certain amplitude of white noise to a time series, decomposing it via EMD, and saving the result. In contrast to the EEMD method, the CEEMD also ensures that the IMF set is quasi-complete and orthogonal. The CEEMD can ameliorate mode mixing and intermittency problems. The CEEMD is a computationally expensive algorithm and may take significant time to run.

3. We all known the complexity of the marine environment, I suggest you can list which factors can make predicting the sea surface temperature more difficult. And these factors can also be added in your simulation.

Response: Thank you for the professional comment. Indeed, when we used empirical orthogonal function descriptions of the spatial structure in this study, it is found that SST variability is spatially complex (being spread over many spatial modes, some of which have small-scale changes) but is dominated by low-frequency changes. The use of linear statistical estimators to examine predictability is discussed and the importance of limiting the number of candidate data used in a correlation search is underscored. Using linear statistical predictors, it is found that SST anomalies can be predicted from SST observations several months in advance with measurable skill. We have stated some factors affecting the SST prediction in the revised manuscript.

Hybrid improved EMD-BPNN model for the prediction of sea surface temperature

Zhiyuan Wu^{a,b,c}, Changbo Jiang^{a,c,*}, Mack Conde^d, Bin Deng^{a,c}, Jie Chen^{a,c}

a. School of Hydraulic Engineering, Changsha University of Science & Technology, Changsha, 410004, China;

b. School for Marine Science and Technology, University of Massachusetts Dartmouth, New Bedford, MA 02744, USA;

c. Key Laboratory of Water-Sediment Sciences and Water Disaster Prevention of Hunan Province, Changsha, 410004, China;

d. Department of Mathematics, University of Massachusetts Dartmouth, North Dartmouth, MA 02747, USA.

Highlights

- A novel SST predicting method based on the hybrid ~~improved~~-EMD algorithms and BP neural network method are proposed in this paper.
- SST prediction results based on the hybrid EEMD-BPNN and CEEMD-BPNN models are compared and discussed.
- Cases study of SST in the North Pacific shows that the proposed hybrid CEEMD-BPNN model can effectively predict the time-series SST.

Abstract: Sea surface temperature (SST) is the major factor that affects the ocean-atmosphere interaction, and in turn the accurate prediction of SST is the key to ocean dynamic prediction. In this paper, an SST predicting method based on ~~improved~~-empirical mode decomposition (EMD) algorithms and back-propagation neural network (BPNN) is proposed. Two different EMD algorithms have been applied extensively for analyzing time-series SST data and some nonlinear stochastic signals. Ensemble empirical mode decomposition (EEMD) algorithm and Complementary Ensemble Empirical Mode Decomposition (CEEMD) algorithm are two improved algorithms of EMD, which can effectively handle the mode-mixing problem and decompose the original data into more stationary signals with different frequencies. Each Intrinsic Mode Function (IMF) has been taken as an input data to the back-propagation neural network model. The final predicted SST data is obtained by aggregating the predicted data of individual IMF. A case study, of the monthly mean sea surface temperature anomaly (SSTA) in the northeastern region of the North Pacific, shows that the proposed hybrid CEEMD-BPNN model is much more accurate than the hybrid EEMD-BPNN model, and the prediction accuracy based on BP neural network is improved by the CEEMD method. Statistical analysis of the case study demonstrates that applying the proposed hybrid CEEMD-BPNN model

30 is effective for the SST prediction.

31

32 **Keywords.**

33 Sea Surface Temperature; Back-Propagation Neural Network; Empirical Mode Decomposition; Prediction;
34 Machine Learning Algorithms.

35

36 **1 Introduction**

37 The Sea Surface Temperature (SST) is a main factor in the interaction between the ocean and the
38 atmosphere (Wiedermann et al., 2017; He et al., 2017; Wu et al., 2019a), and it characterizes the combined
39 results of ocean heat (Buckley et al., 2014; Griffies et al., 2015; Wu et al., 2019b), dynamic processes
40 (Takakura et al., 2018). It is a very important parameter for climate change and ocean dynamics process,
41 reflects sea-air heat and water vapor exchange. Small changes in sea temperature can have a huge impact on
42 the global climate. The well-known El Niño and La Niña phenomena are caused by abnormal changes in SST
43 (Chen et al., 2016a; Zheng et al., 2016).

44 Therefore, scholars have begun to observe the SST in recent years, the observation of the SST is
45 important (Kumar et al., 2017; Sukresno et al., 2018). Accurate observation and effective prediction of the
46 SST are very important (Hudson et al., 2010). Predicting the SST in advance can enable people to take
47 appropriate measures to reduce the impact on daily life and reduce unnecessary losses. However, due to the
48 high randomness of the monthly mean sea surface temperature anomaly (SSTA), the nonlinear and non-
49 stationary characteristics are obvious. At present, there is no clear and feasible method with high accuracy to
50 effectively predict the SST (Zhu et al., 2015; Chen et al., 2016b; Khan et al., 2017).

51 In mathematics and science, a nonlinear system is a system in which the change of the output is not
52 proportional to the change of the input. Nonlinear dynamical systems, describing changes in variables over
53 time, may appear chaotic, unpredictable, or counterintuitive, contrasting with much simpler linear systems.
54 A stationary process is a stochastic process whose unconditional joint probability distribution does not change
55 when shifted in time. Consequently, statistical parameters such as mean and variance also do not change over
56 time. The variation of SST is a deterministic non-linear dynamic system and a non-stationary time series data.
57 ~~The observation sequence at a certain point contains not only the information of this point, but also the~~
58 ~~information of other relevant points.~~ Empirical Mode Decomposition (EMD) is a state-of-the-art signal
59 processing method proposed by Huang et al. (1998). This method can decompose the signal data of different

60 frequencies step by step according to the characteristics of the data and obtain several periodic and trending
61 signals orthogonal to each other, ~~which the method~~ can decompose the stronger nonlinear and non-stationary
62 signals ~~into weaker nonlinear and non-stationary signals~~ (Wang et al., 2015; Amezquita-Sanchez and
63 Adeli, 2015; Wang et al., 2016; Kim and Cho, 2016). The empirical mode decomposition (EMD) method is
64 powerful and adaptive in analyzing nonlinear and non-stationary data sets. It provides an effective approach
65 for decomposing a signal into a collection of so-called intrinsic mode functions (IMFs), which can be treated
66 as empirical basis functions (Duan et al., 2016). However, there were some problems of the EMD method,
67 such as mode mixing (Huang and Wu, 2008; Wu et al., 2008; Wu and Huang, 2009).

68 Once an intermittent signal appears in the actual signal, the EMD decomposition method will produce
69 a Mode Mixing Problem. The Mode Mixing Problem causes the essential modal function to lose its physical
70 meaning. In addition, the Mode Mixing Problem will also make the algorithm of Empirical Mode
71 Decomposition unstable, and any disturbance may generate a new intrinsic mode function. In order to solve
72 this problem, scholars have proposed the use of noise-assisted processing methods, Ensemble empirical mode
73 decomposition (EEMD) and Complementary Ensemble Empirical Mode Decomposition (CEEMD). The
74 white noise has been added to the original signal to change the extreme point distribution of the signal in the
75 EEMD method, while in the CEEMD method, a set of noise signals have been added to the original signal to
76 change the extreme point distribution of the signal.

77 To solve this problem, Wu and Huang (2009) proposed the Ensemble Empirical Mode Decomposition
78 (EEMD) method by adding different white noise in each ensemble member to suppress mode mixing. Yeh et
79 al. (2010) added two opposite-signal white noises to the time-series data sequence, and proposed an improved
80 algorithm for EEMD, Complete Ensemble Empirical Mode Decomposition (CEEMD). The decomposition
81 effect is equivalent to EEMD, and the reconstruction error caused by adding white noise is reduced (Tang et
82 al., 2015). At present, the EMD model and its improved algorithms had been widely used in many fields on
83 ocean science, such as storm surge and sea level rise (Wu et al., 2011; Lee, 2013; Ezer and Atkinson, 2014),
84 tidal amplitude (Cheng et al., 2017; Pan et al., 2018) and wave height (Duan et al., 2016; Sadeghifar et al.,
85 2017; López et al., 2017). These studies and applications reflected that the EMD model and its improved
86 algorithms can effectively reduce the non-stationarity of the time-series data, which helps further analysis
87 and processing.

88 The ensemble empirical mode decomposition (EEMD) method is a noise assisted empirical mode
89 decomposition algorithm. The CEEMD works by adding a certain amplitude of white noise to a time series,

90 decomposing it via EMD, and saving the result. In contrast to the EEMD method, the CEEMD also ensures
91 that the IMF set is quasi-complete and orthogonal. The CEEMD can ameliorate mode mixing and
92 intermittency problems. The CEEMD is a computationally expensive algorithm and may take significant
93 time to run.

94 For nonlinear prediction, the more commonly used methods are curve fitting (Motulsky and Ransnas,
95 1987), gray-box model (Pearson and Pottmann, 2000), homogenization function model (Monteiro et al.,
96 2008), neural network (Deo et al., 2001; Wang et al, 2015; Kim et al., 2016) and so on. Among them, Back-
97 Propagation Neural Network (BPNN) (Lee, 2004; Jain and Deo, 2006; Savitha and Al, 2017; Wang et al.,
98 2018) has certain advantages in dealing with nonlinear problems, it is a basic machine learning algorithm
99 and its principle is simple and operability is strong, so in ocean science and engineering it has been widely
100 used.

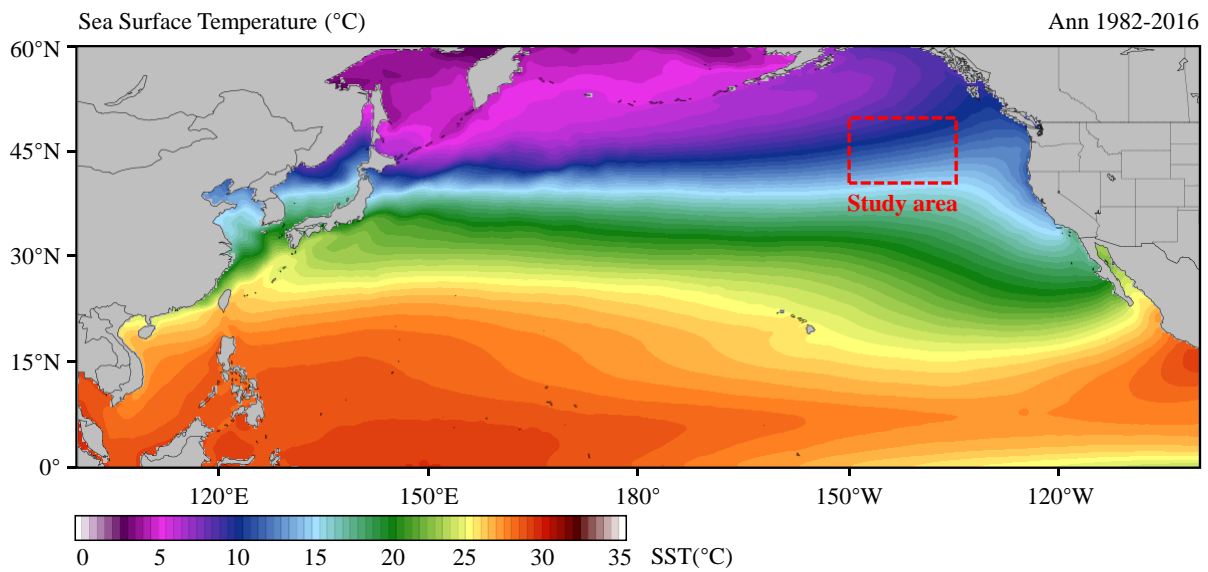
101 In view of non-stationary and nonlinear monthly mean SST, the EEMD, CEEMD and BP neural network
102 will be used here to study how to improve the accuracy of SST prediction. The ~~improved~~ hybrid EMD-BPNN
103 models will be established for the prediction of SSTA in the northeastern region of the Pacific Ocean.

106 **2 Data collection**

107 The SST time-series data in this study is from NOAA Optimum Interpolation Sea Surface Temperature
108 (OISST) official website (Reynolds et al., 2007; Banzon et al., 2016; [https://www.ncdc.noaa.gov/oisst/data-](https://www.ncdc.noaa.gov/oisst/data-access)
109 [access](https://www.ncdc.noaa.gov/oisst/data-access)). The NOAA 1/4°daily OISST is an analysis constructed by combining observations from different
110 platforms (satellites, ships, buoys) on a regular global grid. There are two kinds of OISST, named after the
111 relevant satellite SST sensors. These are the Advanced Very High Resolution Radiometer (AVHRR) and
112 Advanced Microwave Scanning Radiometer on the Earth Observing System (AMSR-E); the AVHRR dataset
113 is used in this study. The average annual sea surface temperature in North Pacific (0°N-60°N, 100°E-100°W)
114 ~~from~~during January 1982 to December 2016 is shown in Fig.1.

115 It has been shown that the sea surface temperature anomaly in the northeastern Pacific in the ten years
116 2006-2016 was 2.0°C warmer than in the previous ten years 1996-2006. Previous studies (Bond et al., 2015)
117 showed that in the spring and summer of 2014, the high SST area of the northeastern Pacific had expanded
118 to coastal ocean waters, which affected the weather in coastal areas and the lives of fishermen, and even
119 affected the temperature in Washington, USA, causing interference to daily life.

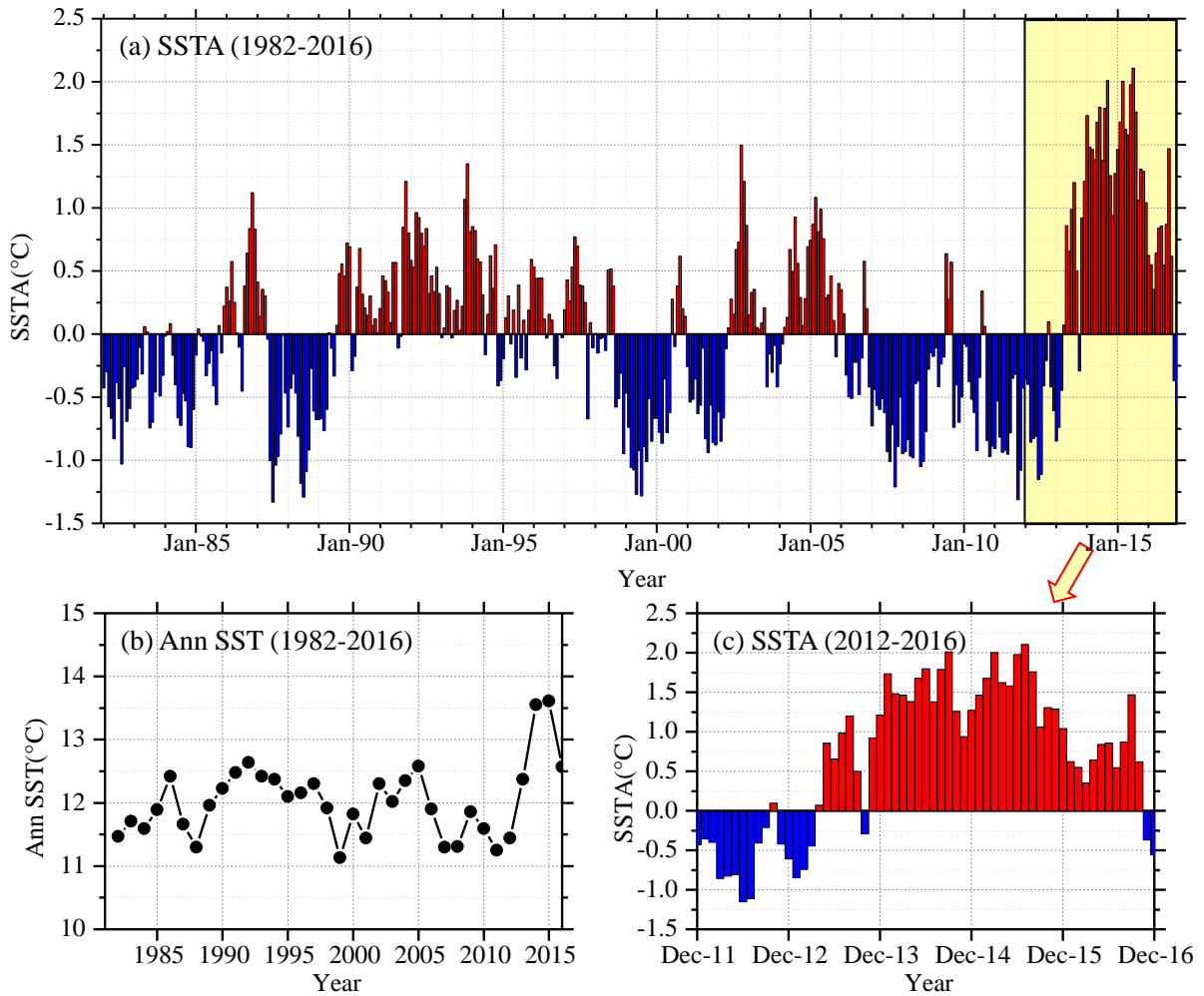
120 In this study, we select the northeastern region of the North Pacific Ocean (in Fig.1, 40°N-50°N, 150°W-
121 135°W) to measure sea surface temperature. The time-series data of SST for the study area from January
122 1982 to December 2016 with a data length of 420 months was obtained from OISST-V2 (Fig. 2). The monthly
123 mean sea surface temperature anomaly (SSTA) was used in the analysis and calculation. As shown in Fig.
124 2(a), it can be found the overall time-series data is very messy, nonlinear and random from the perspective
125 of the image.



127
128 **Fig.1** Average annual sea surface temperature in North Pacific during Jan 1982 to Dec 2016 (35-years).

129
130 ~~It had been shown that the sea surface temperature anomaly in the northeastern Pacific is much hotter~~
131 ~~2.0 °C than that in previous years from the observations in recent ten years (2006-2016). Previous studies~~
132 ~~(Bond et al., 2015) showed that in the spring and summer of 2014, the high SST area of the northeastern~~
133 ~~Pacific had expanded to coastal ocean waters, which affected the weather in coastal areas and the lives of~~
134 ~~fishermen, and even affected the temperature in Washington, USA, the daily life had been caused interference.~~

135 In this study, we select the northeastern region of the North Pacific Ocean (in Fig.1, 40°N-50°N, 150°W-
136 135°W) to measure sea surface temperature. The time-series data of SST for the study area from January
137 1982 to December 2016 with a data length of 420 months was obtained from OISST-V2 (Fig. 2). The monthly
138 mean sea surface temperature anomaly (SSTA) was used in the analysis and calculation. As shown in Fig.
139 2(a), it can be found the overall time-series data is very messy, nonlinear and random from the perspective
140 of the image.



142

143 **Fig.2** The time-series of sea surface temperature in the study area. (a) SSTA anomaly (1982-2016, 35 years);
 144 (b) Annual SSTA (1982-2016, 35 years); (c) SSTA anomaly (2012-2016, 5 years).

145

146 3 Decomposition of SSTA

147 The purpose of this study is to combine the EEMD algorithm and the CEEMD decomposition algorithm
 148 respectively with the BP neural network algorithm to establish a **new** prediction model, an **improved** hybrid
 149 EMD-BPNN model. The EEMD and CEEMD algorithms are performed on the monthly mean SSTA data to
 150 obtain a series of intrinsic mode functions (IMFi). Each IMFi is predicted by a BP neural network and then
 151 each IMFi is reconstructed to obtain the predicted value of SSTA.

152 3.1 Decomposition by the EEMD algorithm

153 The SSTA in Fig. 2(a) has been decomposed based on the ensemble empirical mode decomposition
 154 (EEMD algorithm), and seven IMF components and a residual component RES (Residue) are obtained as

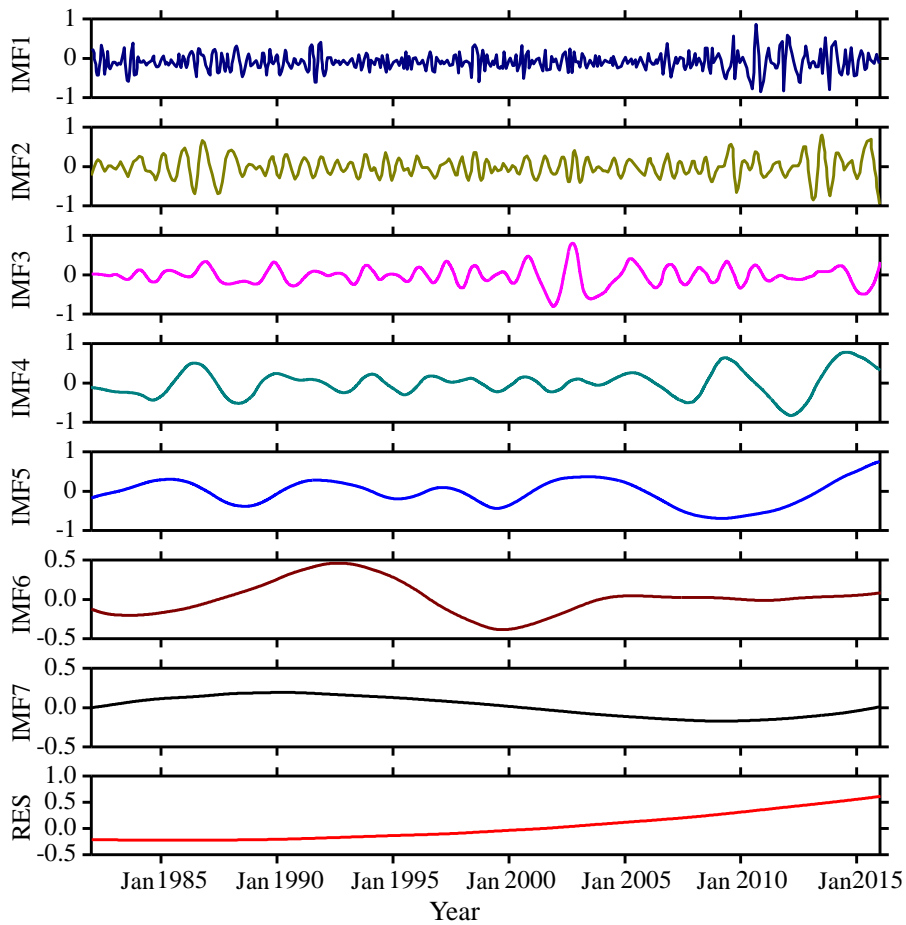
155 shown in Fig. 3.

156 It can be seen from Fig. 3 that the first three intrinsic mode function components IMF1, IMF2, and IMF3
157 still exhibit strong nonlinearity and non-stationarity. The IMF4 to IMF7 and the final trend term RES have
158 some periodicity and relatively regular volatility, and the non-stationary and nonlinear properties are less
159 than the first three components. The trend term RES reflects that the overall trend of SSTA has gradually
160 increased since 1982. As the non-stationarity of each IMF i is gradually reduced, the EEMD algorithm will
161 reduce the influence of non-stationarity on prediction. The absolute error (ERR) of the decomposition can
162 be calculated by the following Formula (1).

$$163 \quad a(t) = \left| S(t) - \left[\sum_{i=1}^7 I_i(t) + R(t) \right] \right| \quad (1)$$

164 where, $a(t)$ is the absolute error (ERR), $S(t)$ the original SSTA observation data, $I_i(t)$ the i -th component
165 of the IMF (IMF i), and $R(t)$ the trend term (RES).

166



167

168 **Fig.3** IMF components and the trend item RES of monthly mean SSTA over the study area based on the

169 EEMD algorithm during 1982-2016.

170

171 It can be seen from Fig. 3 that the first three intrinsic mode function components IMF1, IMF2, and IMF3
172 still exhibit strong nonlinearity and non-stationarity. The IMF4 to IMF7 and the final trend term RES have
173 some periodicity and relatively regular fluctuation, and the non-stationary and nonlinear properties are less
174 than the first three components. The trend term RES reflects that the overall trend of SSTA has gradually
175 increased since 1982. As the non-stationarity of each IMF_i is gradually reduced, the EEMD algorithm will
176 reduce the influence of non-stationarity on prediction. The absolute error (ERR) of the decomposition can
177 be calculated by the following Formula (1).

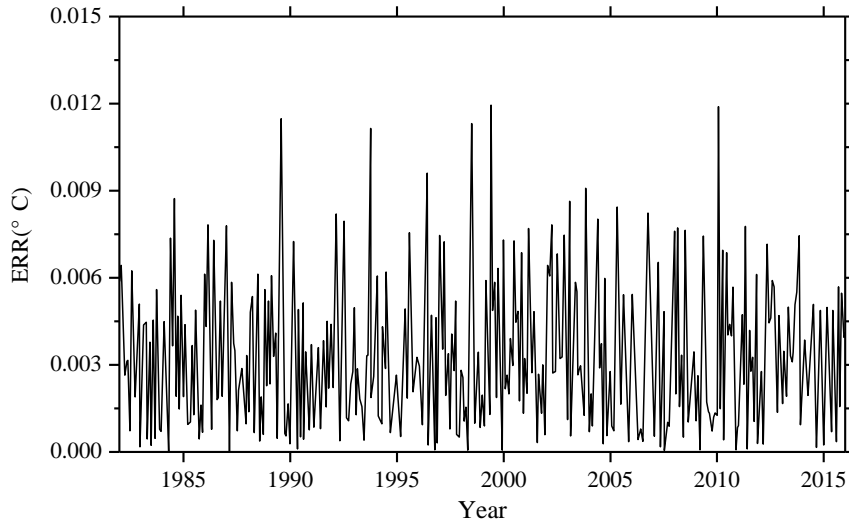
178
$$a(t) = \left| S(t) - \left[\sum_{i=1}^7 I_i(t) + R(t) \right] \right| \quad (1)$$

179 where, $a(t)$ is the absolute error (ERR), $S(t)$ the original SSTA observation data, $I_i(t)$ the i -th component
180 of the IMF (IMF _{i}), and $R(t)$ the trend term (RES).

181 The absolute error (ERR) based on the EEMD algorithm ~~was~~ is shown in Fig. 4. It can be seen from the
182 figure that the ERR of 420 months after decomposition is basically below 0.01 °C, and the ERR ~~–~~exceeds
183 0.01 °C in five months: June 1989, September 1993, July 1998, May 1999 and March 2010.

184 In addition to June 1989, the other four monthly data with a large ERR occurred during the El Niño
185 period. The maximum error is in March 2010, the actual value is -0.1204 °C, the result based on EEMD
186 algorithm is -0.1325 °C, the ERR of decomposition is 0.0121 °C; the minimum error, in April 1987, is
187 1.73×10^{-5} °C. The overall mean ERR based on the EEMD algorithm is 0.0035 °C and the order of magnitude
188 is 10^{-3} .

189



190

191 **Fig. 4** The ERR of monthly mean SSTA over the study area based on the EEMD algorithm during 1982-2016.

192

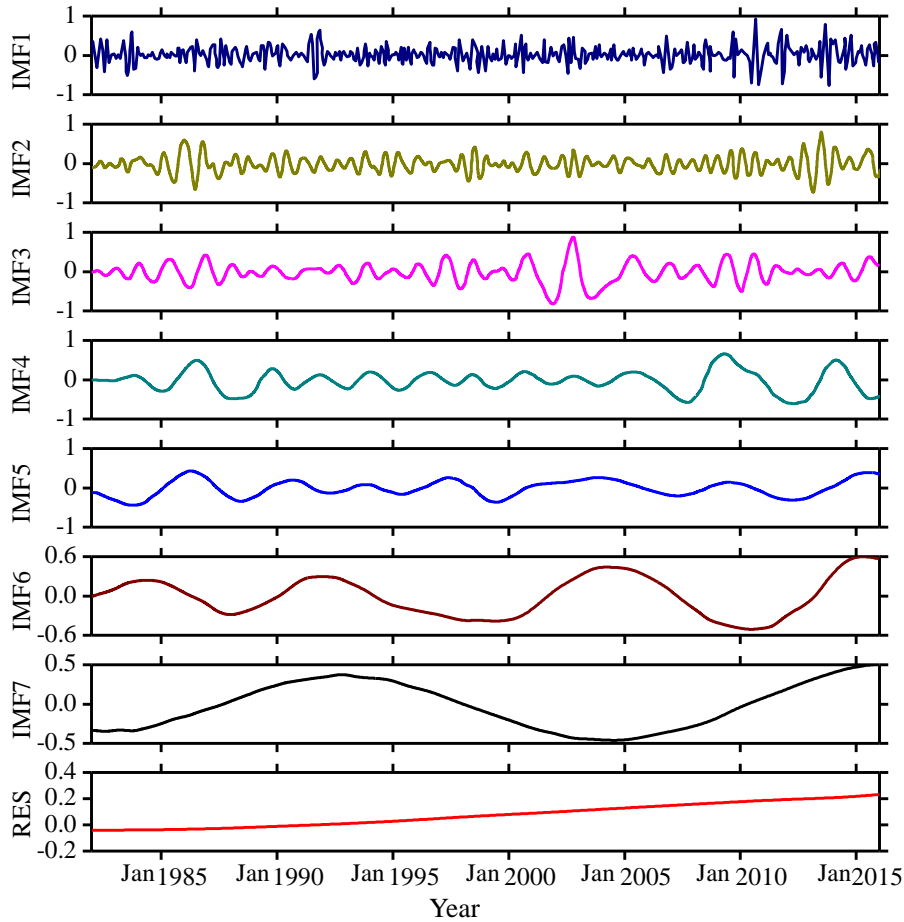
193 ~~In addition to June 1989, the other four monthly data with a large ERR occurred during the El Niño~~
 194 ~~period. The maximum error is in March 2010, the actual value is $-0.1204\text{ }^{\circ}\text{C}$, the result based on EEMD~~
 195 ~~algorithm is $-0.1325\text{ }^{\circ}\text{C}$, the ERR of decomposition is $0.0121\text{ }^{\circ}\text{C}$; the minimum error is in April 1987, which~~
 196 ~~is $1.73 \times 10^{-5}\text{ }^{\circ}\text{C}$. The overall mean ERR based on EEMD algorithm is $0.0035\text{ }^{\circ}\text{C}$ and the order of magnitude~~
 197 ~~is 10^{-3} .~~

198

199 **3.2 Decomposition by the CEEMD algorithm**

200 The SSTA has been decomposed based on the complementary ensemble empirical mode decomposition
 201 (CEEMD algorithm) and seven IMF components and a residual component RES (Residue) are obtained as
 202 shown in Fig. 5. It can be seen when comparing the decomposition results based on EEMD and CEEMD
 203 algorithms that although the mode components decomposed by CEEMD algorithm are different from the
 204 corresponding results decomposed by EEMD, the nonlinearities and non-stationarities of the eight modes
 205 decomposed by the two decomposition algorithms are gradually decreasing, and the final trend term RES is
 206 an upward trend. Both decomposition algorithms confirm the characteristic of a gradual increase ~~infer~~ the
 207 overall trend of the data series.

208



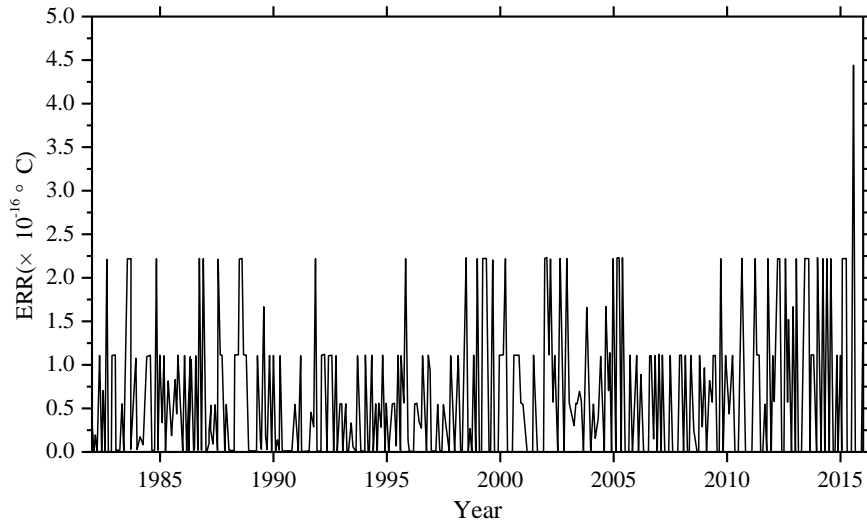
209

210 **Fig.5** IMF components and the trend item RES of monthly mean SSTA over the study area based on the
 211 CEEMD algorithm during 1982-2016.

212

213 The absolute error (ERR) obtained based on the CEEMD algorithm is shown in Fig. 6. It can be seen
 214 from the figure that the ERR of 420 months data after decomposition is less than $5 \times 10^{-16} \text{ }^\circ\text{C}$, and the accuracy
 215 is very better. The maximum error is $4.48 \times 10^{-16} \text{ }^\circ\text{C}$ in March 2016; the minimum error is zero. The overall
 216 mean ERR based on CEEMD algorithm is $6.10 \times 10^{-17} \text{ }^\circ\text{C}$ and the order of magnitude is 10^{-17} . By comparing
 217 the results and errors of the above two decomposition algorithms, it can be seen that the error based on the
 218 improved algorithm (CEEMD) is much smaller than the error based on EEMD algorithm. Because more
 219 white noise with the opposite sign had been added in CEEMD algorithm, the reconstruction error caused
 220 by the white noise has been reduced over it in EEMD algorithm.

221



222

223 **Fig. 6** The ERR of monthly mean SSTA over the study area based on the CEEMD algorithm during 1982-
 224 2016.

225

226 ~~The absolute error (ERR) obtained based on the CEEMD algorithm is shown in Fig. 6. It can be seen~~
 227 ~~from the figure that the ERR of 420 months data after decomposition is less than $5 \times 10^{-16} \text{ }^\circ\text{C}$, and the accuracy~~
 228 ~~is very better. The maximum error is $4.48 \times 10^{-16} \text{ }^\circ\text{C}$ in March 2016; the minimum error is zero. The overall~~
 229 ~~mean ERR based on CEEMD algorithm is $6.10 \times 10^{-17} \text{ }^\circ\text{C}$ and the order of magnitude is 10^{-17} . By comparing~~
 230 ~~the results and errors of the above two decomposition algorithms, it can be seen that the error based on the~~
 231 ~~improved algorithm (CEEMD) is much smaller than the error based on EEMD algorithm. This is because~~
 232 ~~more white noise in CEEMD algorithm had been added than that in EEMD algorithm, so reducing the~~
 233 ~~reconstruction error caused by white noise when the decomposition effect is equivalent to EEMD algorithm.~~

234

235 **4 SSTA prediction model**

236 **4.1 The BP neural network**

237 Artificial Neural Network (ANN) is an information processing approach based on the biological neural
 238 network (López et al., 2015; Kim et al., 2016). In theory, ANN can simulate any complex nonlinear
 239 relationship through nonlinear units (neurons) and has been widely used in the prediction area, such as wave
 240 height and storm surge. The most basic structure of ANN consists of input layers, hidden layers and output
 241 layers. One of the most widely used ANN models is the back propagation neural network (BPNN, Wang et
 242 al., 2018) algorithm based on the BP algorithm.

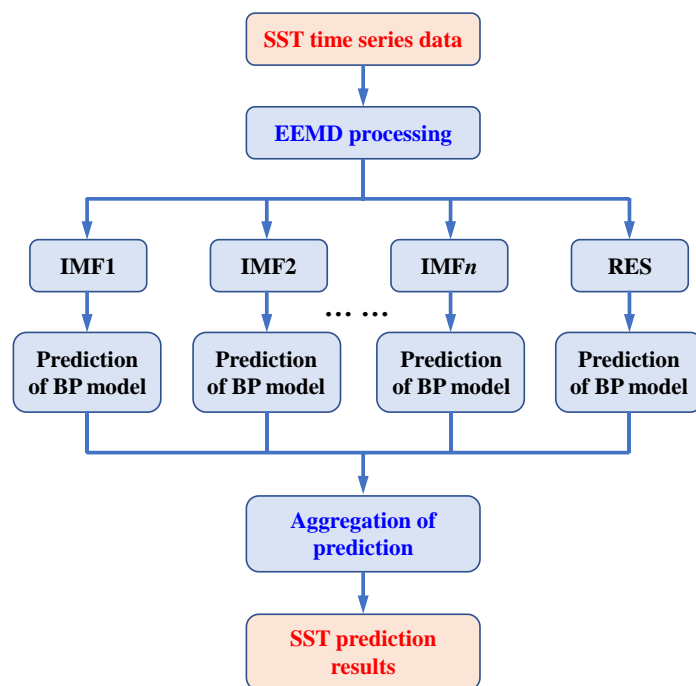
243 The BPNN algorithm is a multi-layer feedforward network trained according to the error back
244 propagation algorithm and is one of the most widely used deep learning algorithms. The BP network can be
245 used to learn and store a large number of mappings of input and output models without the need to publicly
246 describe the mathematical equations of these mapping relationships. The learning rule is to use the steepest
247 descent method. When applied to SST predicting, the input data are monthly mean SST in previous months
248 and the output data are predicted SST time-series data. The desired data for comparison is the observed actual
249 SST.

250

251 **4.2 SSTA prediction model based on hybrid improved EMD-BPNN algorithm**

252 The proposed monthly mean sea surface temperature anomaly (SSTA) predicting model includes three
253 steps as follows. First, original SST datasets are decomposed into certain more stationary signals with
254 different frequencies by EEMD. Second, the BP neural network is used to predict each IMF and the residue
255 RES. A rolling forecasting process is studied. The prediction is made using the previous data for one step
256 ahead. Finally, the prediction results of each IMF and the residue RES are aggregated to obtain the final SST
257 prediction results. The flowchart of the SST prediction model based on hybrid improved empirical mode
258 decomposition algorithm (improved EMD algorithm) and back-propagation neural network (BPNN) is shown
259 in Fig. 7. The SST prediction model has been abbreviated as a hybrid improved EMD-BPNN model in the
260 following article.

261



262
 263 **Fig.7** The flowchart of SST prediction model based on hybrid improved empirical mode decomposition
 264 algorithm (improved EMD algorithm) and back-propagation neural network (BPNN).

265
 266
 267 **5 Case study: SSTA prediction based on the hybrid improved EMD-BPNN models**

268 In order to study the effects of the two improved EMD algorithms (EEMD and CEEMD) on the
 269 prediction results, and to analyze the prediction ability of BP neural network, the following experiments were
 270 carried out. Predict SSTA results in 2017 and analyze the prediction abilities of different mode decomposition
 271 data based on EEMD and CEEMD algorithms. The experiment content is as follows: the BP neural network
 272 is trained with the decomposition data of each mode from 1982 to 2016, and the SSTA in 2017 is predicted
 273 by the trained neural network, and the observation results of 12 months in 2017 ~~areis~~ used to compare and
 274 analyze with the prediction results.

275 Since the nonlinearity of the IMF1 to IMF3 is still relatively strong, a three-layer BP neural network
 276 structure has been chosen and independently analyze and predict each month. For the IMF4 and subsequent
 277 modes, since the nonlinearity and non-stationarity have been degraded relative to the first three modes, a BP
 278 neural network with 12 nodes at input layer and output layer has been used to train and predict SSTA.

279 The prediction results of each mode decomposition component based on the EEMD algorithm are shown
 280 in Fig. 8. The absolute errors of the predicted value and the actual value are shown in Table 1. ~~Root-mean~~

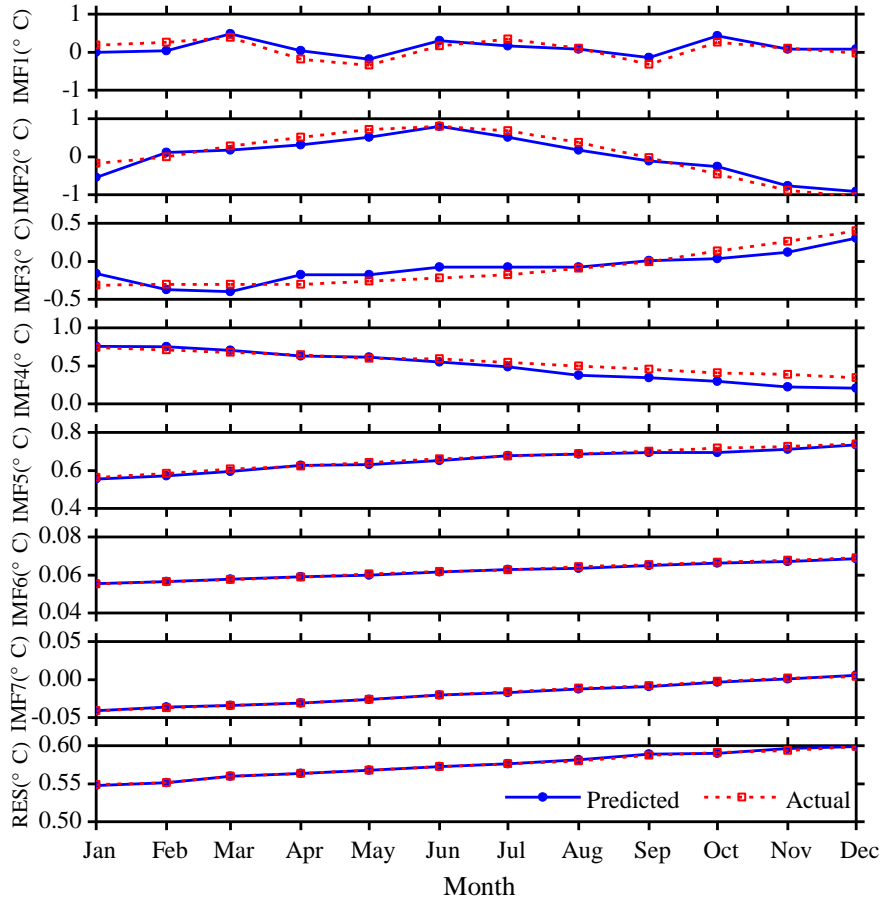
281 square error (RMSE) is used as metrics to access the performance of the two different models.

$$282 \quad \text{RMSE} = \sqrt{\frac{1}{N} \sum_{n=1}^N (x_n - y_n)^2} \quad (2)$$

283 where, x_n and y_n are the observed and the predicted values respectively, N is the number of data used for
284 the performance evaluation. Results are shown in Table 1.

285 It can be seen from Fig. 8 and Table 1 that the maximum absolute error (Max ERR) of the first
286 decomposition component IMF1 based on the hybrid EEMD-BPNN model is 0.2197 °C in January. The
287 minimum absolute error (Min ERR) is 0.0014 °C, which is in August. The prediction ability of the second
288 mode decomposition component IMF2 is roughly equivalent to the IMF1, and the mean absolute error (Mean
289 ERR) of the first three intrinsic mode function components IMF1, IMF2, and IMF3 are between 0.10 °C and
290 0.15 °C. The mean absolute errors of the IMF4 and IMF5 are 0.0663 °C and 0.0089 °C, respectively, and the
291 prediction accuracy based on the hybrid EEMD-BPNN model is roughly equivalent to the decomposition
292 accuracy of the EEMD algorithm. The prediction errors of the last two intrinsic mode function components
293 and the residue RES are on the order of 10^{-4} . It can be seen that as the nonlinearity and non-stationarity of
294 the series data decreases, the error of the prediction results becomes smaller and smaller.

295



296
 297 **Fig. 8** SSTA prediction results based on the hybrid EEMD-BPNN model of each individual component in
 298 2017.

300 Root mean square error (RMSE) is used as metrics to access the performance of the two different models.

$$301 \quad \text{RMSE} = \sqrt{\frac{1}{N} \sum_{n=1}^N (x_n - y_n)^2} \quad (2)$$

302 where, x_n and y_n are the observed and the predicted values respectively, N is the number of data used for
 303 the performance evaluation. Results are shown in Table 1.

305 **Table 1.** The absolute errors ERRs of the SSTA prediction results of each individual component based on the
 306 hybrid EEMD-BPNN model (unit: °C).

	Max ERR	Min ERR	Mean ERR	RMSE
IMF1	0.2197	0.0014	0.1424	0.1486
IMF2	0.2166	0.0323	0.1297	0.1673
IMF3	0.1872	0.0051	0.1070	0.1245

IMF4	0.1602	1.6876869×10^{-4}	0.0663	0.0857
IMF5	0.0158	0.0010	0.0089	0.0104
IMF6	3.8778766×10^{-4}	1.9752×10^{-4}	2.7221×10^{-4}	0.0003
IMF7	5.2662×10^{-4}	1.6396387×10^{-4}	1.7917907×10^{-4}	0.0002
RES	5.4864859×10^{-4}	2.2312308×10^{-4}	2.4774766×10^{-4}	0.0002

307

308

309

310

311

312

313

314

315

316

317

It can be seen from Fig. 8 and Table 1 that the maximum absolute error (Max ERR) of the first decomposition component IMF1 based on the hybrid EEMD-BPNN model is 0.2197 °C in January. The minimum absolute error (Min ERR) is 0.0014 °C, which is in August. The prediction ability of the second mode decomposition component IMF2 is roughly equivalent to the IMF1, and the mean absolute error (Mean ERR) of the first three intrinsic mode function components IMF1, IMF2, and IMF3 are between 0.10 °C and 0.15 °C. The mean absolute errors of the IMF4 and IMF5 are 0.0663 °C and 0.0089 °C, respectively, and the prediction accuracy based on the hybrid EEMD-BPNN model is roughly equivalent to the decomposition accuracy of the EEMD algorithm. The prediction errors of the last two intrinsic mode function components and the residue RES are on the order of 10^{-4} . It can be seen that as the nonlinearity and non-stationarity of the series data decreases, the error of the prediction results becomes smaller and smaller.

318

319

320

321

322

According to the same method, the eight mode components decomposed by CEEMD algorithm have been analyzed and predicted. The prediction results and error analysis have been shown in Fig. 9 and Table 2. It can be seen from Fig. 9 and Table 2 that the maximum error of the first decomposition component IMF1 based on the hybrid CEEMD-BPNN model is 0.1779 °C in May. The minimum error is 0.0068 °C, which is in June.

323

324

325

326

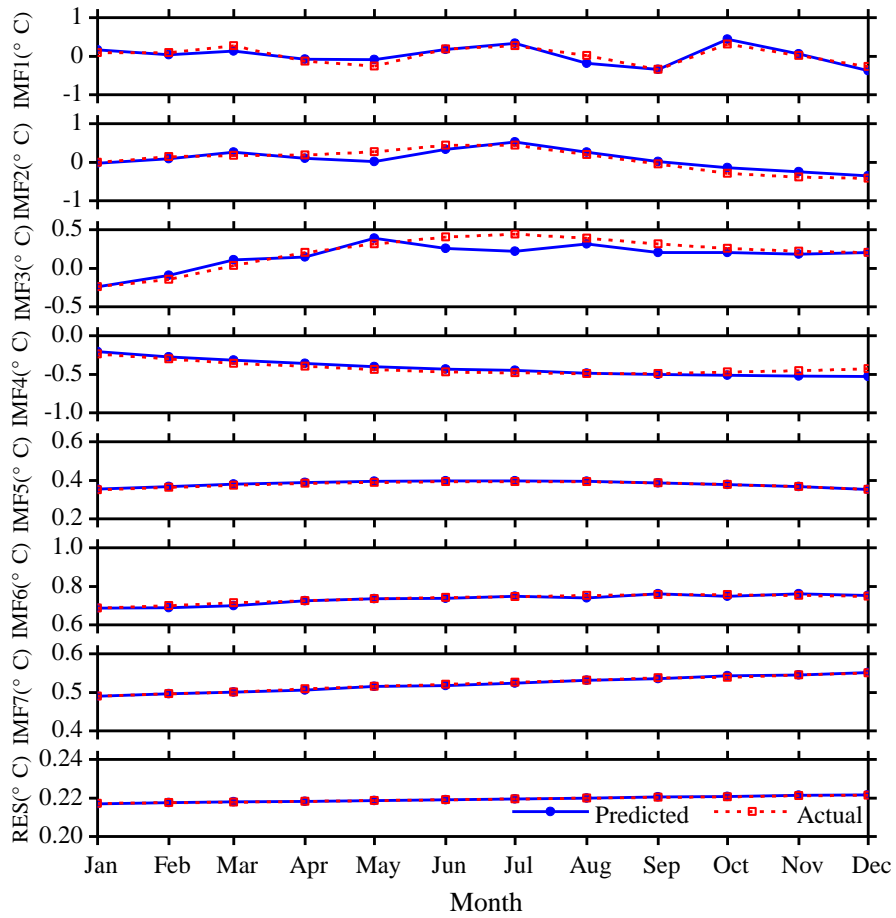
327

328

329

330

The prediction ability of the second mode decomposition component IMF2 is roughly equivalent to the IMF1. Except for the four months of May, September, October, and November, the accuracies of prediction results of other months are satisfactory. The prediction results of the first three intrinsic mode function components IMF1, IMF2, and IMF3 are basically the same as the actual data. In the prediction results of the fourth mode component IMF4, except for slight error in December, the prediction ability is better. The predicted results of the last three intrinsic mode function components IMF5, IMF6, IMF7 and the residue RES are basically consistent with the observation results.



331

332 **Fig. 9** SSTA prediction results based on the hybrid CEEMD-BPNN model of each individual component in

333 2017.

334

335

336 **Table 2.** The absolute errors ERRs of the SSTA prediction results of each individual component based on the
337 hybrid CEEMD-BPNN model (unit: °C).

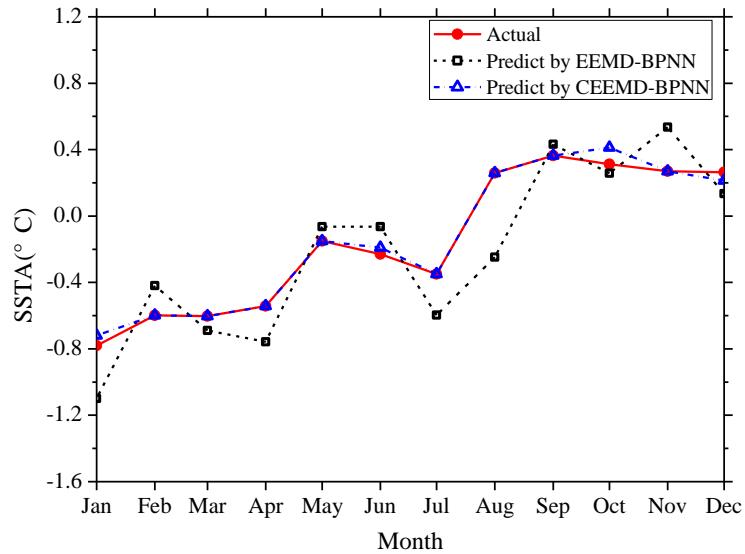
	Max ERR	Min ERR	Mean ERR	RMSE
IMF1	0.1779	0.0068	0.0827	0.0987
IMF2	0.1643	0.0413	0.0811	0.1124
IMF3	0.1521	0.0160	0.0713	0.1006
IMF4	0.0851	0.0211	0.0324	0.0427
IMF5	0.0052	8.7694×10^{-5}	0.0021	0.0029
IMF6	0.0103	5.7757748×10^{-5}	0.0043	0.0056
IMF7	0.0017	3.6036026×10^{-5}	9.1374×10^{-4}	0.0010
RES	3.0342×10^{-5}	2.0163×10^{-6}	1.1572×10^{-5}	1.5025017×10^{-5}

338

339 ~~The prediction ability of the second mode decomposition component IMF2 is roughly equivalent to the~~
340 ~~IMF1. Except for the four months of May, September, October, and November, the accuracies of prediction~~
341 ~~results of other months are satisfactory. The prediction results of the first three intrinsic mode function~~
342 ~~components IMF1, IMF2, and IMF3 are basically the same as the actual data. In the prediction results of the~~
343 ~~fourth mode component IMF4, except for slight error in December, the prediction ability is better. The~~
344 ~~predicted results of the last three intrinsic mode function components IMF5, IMF6, IMF7 and the residue~~
345 ~~RES are basically consistent with the observation results.~~

346 The prediction results of the monthly mean SSTA in 2017 are obtained by reconstructing the mode
347 decomposition components (Fig. 10) and the absolute error (ERR) of prediction results has been shown in
348 Table 3. It can be seen from the figure and table that the prediction results based on the EEMD-BPNN model
349 have larger ERRs in January and August, exceeding 0.3 °C, and the accuracies of prediction results in other
350 months are satisfactory (the ERR is less than 0.3). The prediction accuracy based on the CEEMD-BPNN
351 model is satisfactory, except for the ERR exceeding 0.1 °C in October, and the prediction ability based on
352 the CEEMD-BPNN model is generally better than that of the EEMD-BPNN model.

353



354
355 **Fig. 10** Monthly SSTA prediction results based on the hybrid improved EMD-BPNN models in 2017.

356
357
358 **Table 3.** The absolute errors ERRs of the SSTA prediction results based on the two different hybrid improved
359 EMD-BPNN models (unit: °C).

	EEMD-BPNN model	CEEMD-BPNN model		EEMD-BPNN model	CEEMD-BPNN model
Jan	0.3188	0.0623	Sep	0.0687	0.0132
Feb	0.1780	0.0103	Oct	0.0545	0.1607
Mar	0.0867	0.0063	Nov	0.2651	0.0101
Apr	0.2153	0.0137	Dec	0.1290	0.0183
May	0.0854	0.0102	Min ERR	0.0545	0.0063
Jun	0.1662	0.0224	Max ERR	0.5068	0.1607
Jul	0.2474	0.0077	Mean ERR	0.1935	0.0289
Aug	0.5068	0.0112	RMSE	0.2299	0.0512

360
361 The prediction values based on the CEEMD-BPNN model and the observation values at the significance
362 level of 0.001, the correlation coefficient reached 0.97Correlation coefficient between the prediction values
363 based on the CEEMD-BPNN model and observations is shown that the value of the correlation coefficient
364 that indicates a significance level of 0.001 and the correlation coefficient reached 0.97.; The result which
365 indicates that SSTA in 2017 had been predicted accurately by the CEEMD-BPNN model. As can be seen

366 from the above discussions, the ERR of decomposition components based on the EEMD and CEEMD
367 algorithms will affect the accuracy of the final prediction results. Table 3 shows that predicting results of the
368 hybrid CEEMD and BPNN model are ameliorated a lot as compared to the EEMD-BPNN direct predicting
369 model. This is because after CEEMD, the original unsteady and nonlinear data are changed into certain
370 components that have fixed frequency and periodicity. The CEEMD algorithm with less decomposition error
371 has less error in the final prediction results, which proves that the CEEMD method has more advantages in
372 data decomposition than the EEMD method. At the same time, we can find that the final prediction error of
373 the two prediction models mainly comes from the first three mode decomposition components, and the error
374 of the last five components has little effect on the accuracy of the final prediction results.

375

376 6 Conclusions

377 This paper presents a ~~novel~~ SST predicting method based on the hybrid ~~improved~~ EMD algorithms and
378 BP neural network method to process the SST data with ~~strong~~ nonlinearity and non-stationarity. Through
379 EEMD and CEEMD algorithms, SSTA time-series data are decomposed into different IMFs and a residue
380 RES. BP neural network is applied to predict individual IMFs and the residue RES. Final results can be
381 obtained by adding the predicting results of individual IMFs and RES.

382 In order to illustrate the effectiveness of the proposed approach, a case study was carried out. SSTA
383 ~~prediction~~ results based on the hybrid EEMD-BPNN model and ~~the~~ hybrid CEEMD-BPNN model
384 are discussed respectively. In comparison, the proposed hybrid CEEMD-BPNN model is much better and its
385 prediction results are more accurate.

386 From the absolute error of the prediction results of each component IMF and the absolute error of the
387 predicted SSTA, the prediction error of SSTA mainly comes from the prediction of the first three mode
388 decomposition component (IMF1, IMF2 and IMF3), because the first three mode components still have
389 strong nonlinearity and non-stationarity. As the nonlinearity gradually decreases, the absolute error of the
390 prediction results gradually decreases.

391 SST prediction has been only preliminary carried out based on the two improved EMD algorithms and
392 BP neural network in this paper. The results show that the hybrid CEEMD-BPNN model is more accurate in
393 predicting SST. This work can provide a reference for predicting SST and El Niño in the future. In the follow-
394 up study, how to improve the forecast duration is the focus of this work.

395

396 **Acknowledgement**

397 This work was supported by National Natural Science Foundation of China (Grant Nos. 51809023,
398 51879015, 51839002, 51809021 and 51509023).

399

400 **References:**

401 Amezquita-Sanchez, J. P. and Adeli, H.: A new music-empirical wavelet transform methodology for time–
402 frequency analysis of noisy nonlinear and non-stationary signals, *Digit. Signal Process.*, 45, 55-68,
403 <https://doi.org/10.1016/j.dsp.2015.06.013>, 2015.

404 Banzon, V., Smith, T. M., Chin, T. M., Liu, C., and Hankins, W.: A long-term record of blended satellite and
405 in situ sea-surface temperature for climate monitoring, modeling and environmental studies, *Earth Syst.*
406 *Sci. Data*, 8, 165-176, <https://doi.org/10.5194/essd-8-165-2016>, 2016.

407 Bond, N. A., Cronin, M. F., Freeland, H., and Mantua N.: Causes and impacts of the 2014 warm anomaly in
408 the NE Pacific. *Geophys. Res. Lett.*, 42, 3414-3420, <https://doi.org/10.1002/2015GL063306>, 2015.

409 Buckley, M. W., Ponte, R. M., Forget, G., and Heimbach, P.: Low-frequency SST and upper-ocean heat
410 content variability in the North Atlantic, *J. Climate*, 27, 4996-5018, [https://doi.org/10.1175/JCLI-D-13-](https://doi.org/10.1175/JCLI-D-13-00316.1)
411 [00316.1](https://doi.org/10.1175/JCLI-D-13-00316.1), 2014.

412 Chen, C., Cane, M. A., Henderson, N., Lee, D. E., Chapman, D., Kondrashov D., and Chekroun, M. D.:
413 Diversity, nonlinearity, seasonality, and memory effect in ENSO simulation and prediction using
414 empirical model reduction, *J. Climate*, 29: 1809-1830, <https://doi.org/10.1175/JCLI-D-15-0372.1>,
415 2016b.

416 Chen, Z., Wen, Z., Wu, R., Lin X., and Wang J.: Relative importance of tropical SST anomalies in maintaining
417 the Western North Pacific anomalous anticyclone during El Niño to La Niña transition years, *Clim.*
418 *Dynam.*, 46, 1027-1041, <https://doi.org/10.1007/s00382-015-2630-1>, 2016a.

419 Cheng, Y., Ezer, T., Atkinson, L. P., and Xu, Q.: Analysis of tidal amplitude changes using the EMD method,
420 *Cont. Shelf Res.*, 148: 44-52, <https://doi.org/10.1016/j.csr.2017.09.009>, 2017.

421 Deo, M. C., Jha, A., Chaphekar, A. S., and Ravikant, K.: Neural networks for wave forecasting, *Ocean Eng.*,
422 28: 889-898, [https://doi.org/10.1016/S0029-8018\(00\)00027-5](https://doi.org/10.1016/S0029-8018(00)00027-5), 2001.

423 Duan, W. Y., Han, Y., Huang, L. M., Zhao, B. B., and Wang, M. H.: A hybrid EMD-SVR model for the short-
424 term prediction of significant wave height, *Ocean Eng.*, 124, 54-73,
425 <https://doi.org/10.1016/j.oceaneng.2016.05.049>, 2016.

426 Duan, W., Huang, L., Han Y., and Huang D.: A hybrid EMD-AR model for nonlinear and non-stationary
427 wave forecasting, J Zhejiang Univ-Sc A, 17(2): 115-129, <https://doi.org/10.1631/jzus.A1500164>, 2016.

428 Ezer, T. and Atkinson, L. P.: Accelerated flooding along the US East Coast: on the impact of sea - level rise,
429 tides, storms, the Gulf Stream, and the North Atlantic oscillations, *Earths Future*, 2, 362-382,
430 <https://doi.org/10.1002/2014EF000252>, 2014.

431 Griffies, S. M., Winton, M., Anderson, W. G., Benson, R., Delworth, T. L., Dufour, C. O., Dunne, J. P.,
432 Goddard, P., Morrison, A. K., Rosati, A., Wittenberg, A. T., Yin, J., and Zhang, R.: Impacts on ocean
433 heat from transient mesoscale eddies in a hierarchy of climate models. *J. Climate*, 28, 952-977,
434 <https://doi.org/10.1175/JCLI-D-14-00353.1>, 2015.

435 He, J., Deser, C., and Soden, B. J.: Atmospheric and oceanic origins of tropical precipitation variability. *J.*
436 *Climate*, 30, 3197-3217, <https://doi.org/10.1175/JCLI-D-16-0714.1>, 2017.

437 Huang, N. E., Shen, Z., Long, S. R., Wu, M. C., Shih, H. H., Zheng, Q., Yen, N., Tung, C. C., and Liu, H. H.:
438 The empirical mode decomposition and the Hilbert spectrum for nonlinear and non-stationary time
439 series analysis, *P. Roy. Soc. A-Math. Phys.*, 454, 903-995. <https://doi.org/10.1098/rspa.1998.0193>, 1998.

440 Huang, N. E. and Wu, Z.: A review on Hilbert - Huang transform: Method and its applications to geophysical
441 studies, *Rev. Geophys.*, 46, RG2006, <https://doi.org/10.1029/2007RG000228>, 2008.

442 Hudson, D., Alves, O., Hendon, H. H., Wang, G.: The impact of atmospheric initialisation on seasonal
443 prediction of tropical Pacific SST, *Clim. Dynam.*, 36, 1155-1171, [https://doi.org/10.1007/s00382-010-](https://doi.org/10.1007/s00382-010-0763-9)
444 [0763-9](https://doi.org/10.1007/s00382-010-0763-9), 2011.

445 Jain, P. and Deo, M. C.: Neural networks in ocean engineering, *Ships Offshore Struc.*, 1, 25-35,
446 <https://doi.org/10.1533/saos.2004.0005>, 2006.

447 Khan, M. Z. K., Sharma, A., and Mehrotra, R.: Global seasonal precipitation forecasts using improved sea
448 surface temperature predictions, *J Geophys. Res. -Atmos.*, 122, 4773-4785,
449 <https://doi.org/10.1002/2016JD025953>, 2017,

450 Kim, Y., Kim, H., and Ahn, I. G.: A study on the fatigue damage model for Gaussian wideband process of
451 two peaks by an artificial neural network, *Ocean Eng.*, 111, 310-322,
452 <https://doi.org/10.1016/j.oceaneng.2015.11.008>, 2016.

453 Kumar, M., Parmar, C., Chaudhary, V., Kumar, A., and SST-1 team.: Observation of plasma shift in SST-1
454 using optical imaging diagnostics, *J Phys. Conf. Ser.*, 823, 012056, [https://doi.org/10.1088/1742-](https://doi.org/10.1088/1742-6596/823/1/012056)
455 [6596/823/1/012056](https://doi.org/10.1088/1742-6596/823/1/012056), 2017.

456 Lee, H. S.: Estimation of extreme sea levels along the Bangladesh coast due to storm surge and sea level rise
457 using EEMD and EVA, *J Geophys. Res.-Oceans*, 118, 4273-4285, <https://doi.org/10.1002/jgrc.20310>,
458 2013,

459 Lee, T. L.: Back-propagation neural network for long-term tidal predictions, *Ocean Eng.*, 31, 225-238,
460 [https://doi.org/10.1016/S0029-8018\(03\)00115-X](https://doi.org/10.1016/S0029-8018(03)00115-X), 2004.

461 López, I., Aragonés, L., Villacampa, Y., and Serra, J. C.: Neural network for determining the characteristic
462 points of the bars, *Ocean Eng.*, 136: 141-151, <https://doi.org/10.1016/j.oceaneng.2017.03.033>, 2017.

463 Monteiro, E., Yvonnet, J., He, Q. C.: Computational homogenization for nonlinear conduction in
464 heterogeneous materials using model reduction. *Comp. Mater. Sci.*, 42, 704-712,
465 <https://doi.org/10.1016/j.commatsci.2007.11.001>, 2008.

466 Motulsky, H. J. and Ransnas, L. A.: Fitting curves to data using nonlinear regression: a practical and
467 nonmathematical review, *Faseb J.*, 1, 365-374. <https://doi.org/10.1096/fasebj.1.5.3315805>, 1987.

468 Pan, H., Guo, Z., Wang, Y., and Lv, X.: Application of the EMD method to river tides, *J. Atmos. Ocean. Tech.*,
469 35, 809-819, <https://doi.org/10.1175/JTECH-D-17-0185.1>, 2018.

470 Pearson, R. K. and Pottmann, M.: Gray-box identification of block-oriented nonlinear models, *J. Process*
471 *Contr.*, 10, 301-315, [https://doi.org/10.1016/S0959-1524\(99\)00055-4](https://doi.org/10.1016/S0959-1524(99)00055-4), 2000.

472 Reynolds, R. W., Smith, T. M., Liu, C., Chelton, D. B., Casey, K. S., and Schlax., M. G.: Daily high-
473 resolution-blended analyses for sea surface temperature, *J. Climate*, 20, 5473-5496,
474 <https://doi.org/10.1175/2007JCLI1824.1>, 2007.

475 Sadeghifar, T., Motlagh, M. N., Azad, M. T., and Mahdizadeh, M. M.: Coastal wave height prediction using
476 Recurrent Neural Networks (RNNs) in the south Caspian Sea, *Mar. Geod.*, 40, 454-465,
477 <https://doi.org/10.1080/01490419.2017.1359220>, 2017.

478 Savitha, R. and Mamun, A. A.: Regional ocean wave height prediction using sequential learning neural
479 networks, *Ocean Eng.*, 129: 605-612, <https://doi.org/10.1016/j.oceaneng.2016.10.033>, 2017.

480 Sukresno, B., Hanintyo, R., Kusuma, D. W., Jatisworo, D., and Murdimanto., A.: Three-way error analysis
481 of sea surface temperature (SST) between HIMAWARI-8, buoy, and mur SST in SAVU Sea, *Int. J.*
482 *Remote Sens. Earth Sci.*, 15, 25-36, <https://doi.org/10.30536/j.ijreses.2018.v15.a2855>, 2018,

483 Takakura, T., Kawamura, R., Kawano, T., Ichiyangi, K., Tanoue, M., and Yoshimura, K.: An estimation of
484 water origins in the vicinity of a tropical cyclone's center and associated dynamic processes, *Clim.*
485 *Dynam.*, 50, 555-569, <https://doi.org/10.1007/s00382-017-3626-9>, 2018.

- 486 Tang, L., Dai, W., Yu, L., and Wang, S.: A novel CEEMD-based EELM ensemble learning paradigm for crude
487 oil price forecasting, *Int. J. Inf. Tech. Decis.*, 14, 141-169, <https://doi.org/10.1142/S0219622015400015>,
488 2015.
- 489 Wang, S., Zhang, N., Wu, L., and Wang, Y.: Wind speed forecasting based on the hybrid ensemble empirical
490 mode decomposition and GA-BP neural network method, *Renew. Energ.*, 94, 629-636,
491 <https://doi.org/10.1016/j.renene.2016.03.103>, 2016.
- 492 Wang, W., Chau, K., Xu, D., and Chen, X.: Improving forecasting accuracy of annual runoff time series using
493 ARIMA based on EEMD decomposition, *Water Resour. Manag.*, 29, 2655-2675,
494 <https://doi.org/10.1007/s11269-015-0962-6>, 2015.
- 495 Wang, W., Tang, R., Li, C., Liu, P., and Luo, L.: A BP neural network model optimized by Mind Evolutionary
496 Algorithm for predicting the ocean wave heights, *Ocean Eng.*, 162, 98-107,
497 <https://doi.org/10.1016/j.oceaneng.2018.04.039>, 2018.
- 498 Wang, Y., Wilson, P. A., Zhang, M., and Liu, X.: Adaptive neural network-based backstepping fault tolerant
499 control for underwater vehicles with thruster fault, *Ocean Eng.*, 110, 15-24,
500 <https://doi.org/10.1016/j.oceaneng.2015.09.035>, 2015.
- 501 Wiedermann, M., Donges, J. F., Handorf, D., Kurths, J., and Donner, R. V.: Hierarchical structures in
502 Northern Hemispheric extratropical winter ocean–atmosphere interactions, *Int. J. Climatol.*, 37, 3821-
503 3836, <https://doi.org/10.1002/joc.4956>, 2017.
- 504 Wu, L. C., Kao, C. C., Hsu, T. W., Jao K. C. and Wang, Y. F.: Ensemble empirical mode decomposition on
505 storm surge separation from sea level data, *Coast. Eng. J.*, 53, 223-243,
506 <https://doi.org/10.1142/S0578563411002343>, 2011.
- 507 Wu Z., Schneider E. K. and Kirtman B. P.: The modulated annual cycle: an alternative reference frame for
508 climate anomalies, *Clim. Dyna.*, 31(7-8): 823-841, <https://doi.org/10.1007/s00382-008-0437-z>, 2008.
- 509 Wu, Z. and Huang, N. E.: Ensemble empirical mode decomposition: a noise-assisted data analysis method,
510 *Adv. Adap. Data Anal.*, 1, 1-41, <https://doi.org/10.1142/S1793536909000047>, 2009.
- 511 Wu Z., Jiang C., Chen J., Long Y., Deng B. and Liu X.: Three-Dimensional Temperature Field Change in the
512 South China Sea during Typhoon Kai-Tak (1213) Based on a Fully Coupled Atmosphere–Wave–Ocean
513 Model, *Water*, 11(1): 140, <https://doi.org/10.3390/w11010140>, 2019a.
- 514 Wu Z., Jiang C., Deng B., Chen J., Long Y., Qu K. and Liu X.: Numerical investigation of Typhoon Kai-tak
515 (1213) using a mesoscale coupled WRF-ROMS model, *Ocean Eng.*, 175: 1-15.

516 <https://doi.org/10.1016/j.oceaneng.2019.01.053>, 2019b.

517 Yeh, J. R., Shieh, J. S., and Huang, N. E.: Complementary ensemble empirical mode decomposition: A novel
518 noise enhanced data analysis method, *Adv. Adap. Data Anal.*, 2, 135-156,
519 <https://doi.org/10.1142/S1793536910000422>, 2010.

520 Zheng, X. T., Xie, S. P., Lv, L. H., and Zhou, Z. Q.: Intermodel uncertainty in ENSO amplitude change tied
521 to Pacific Ocean warming pattern, *J. Climate*, 29, 7265-7279, <https://doi.org/10.1175/JCLI-D-16-0039.1>,
522 2016.

523 Zhu, J., Huang, B., Kumar, A., and Kinter, J. L.: Seasonality in prediction skill and predictable pattern of
524 tropical Indian Ocean SST, *J. Climate*, 28, 7962-7984, <https://doi.org/10.1175/JCLI-D-15-0067.1>, 2015.

525